IGS 2026 WORKSHOP
SANTIAGO DE CHILE
33°26' S 70°39' O

1-5 June 2026

Manuel Bravo, Carlos Castillo-Rivera, Ignacia Calisto, Juan Gonzalez, Roberto Benavente

UNACH Universidad Adventista de Chile
Agencia Nacional de Investigación y Desarrollo
Ministerio de Ciencia, Tecnología, Conocimiento e Innovación
Gobierno de Chile
DGEO Universidad de Concepción
Universidad Andrés Bello
UCSC
CIGIDEN Research Center for Integrated Disaster Risk Management

GNSS-Based detection of ionospheric disturbances associated with earthquakes, tsunamis, and volcanic eruptions

Ionospheric response to natural hazards

Earthquakes, tsunamis, and volcanic eruptions generate atmospheric acoustic-gravity waves that propagate upward and disturb the ionosphere.

These disturbances can be remotely detected using GNSS observations.

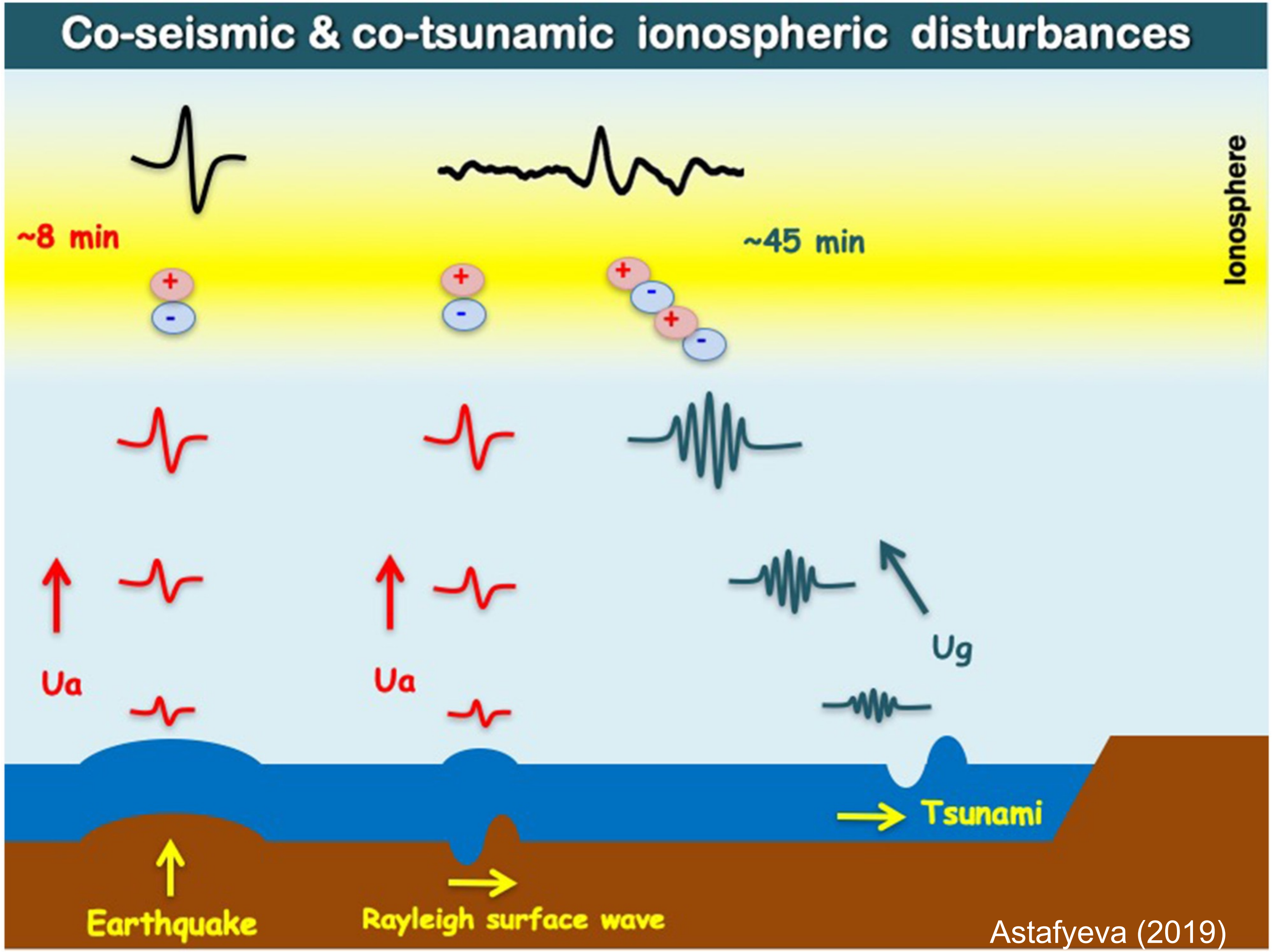

Ionospheric response to natural hazards

Volcanic eruptions can produce strong co-volcanic ionospheric disturbances through the generation of acoustic and gravity waves.

Acoustic and gravity waves are distinguished by characteristic frequency and period ranges.

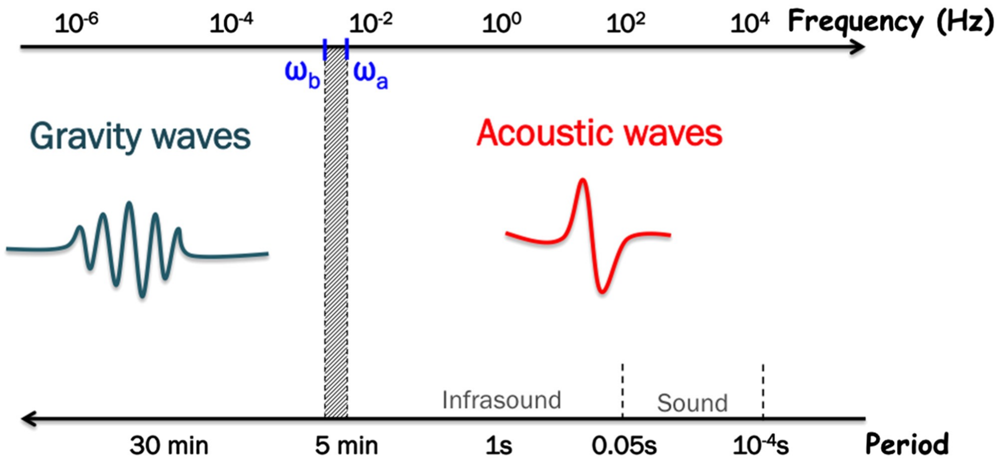

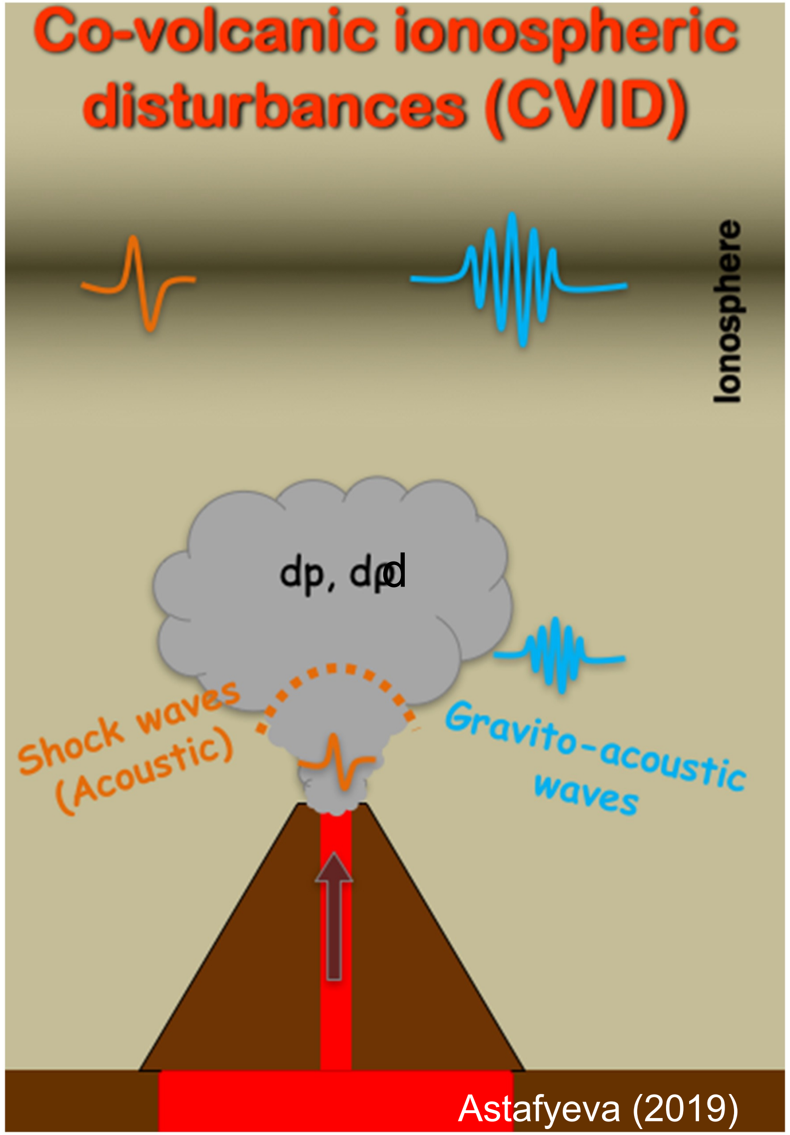

Ionospheric response to natural hazards

But what is the ionosphere?

The ionosphere is a partially ionized region of the upper atmosphere located mainly within the upper mesosphere and thermosphere.

It contains free electrons and ions that affect radio wave propagation and GNSS signals..

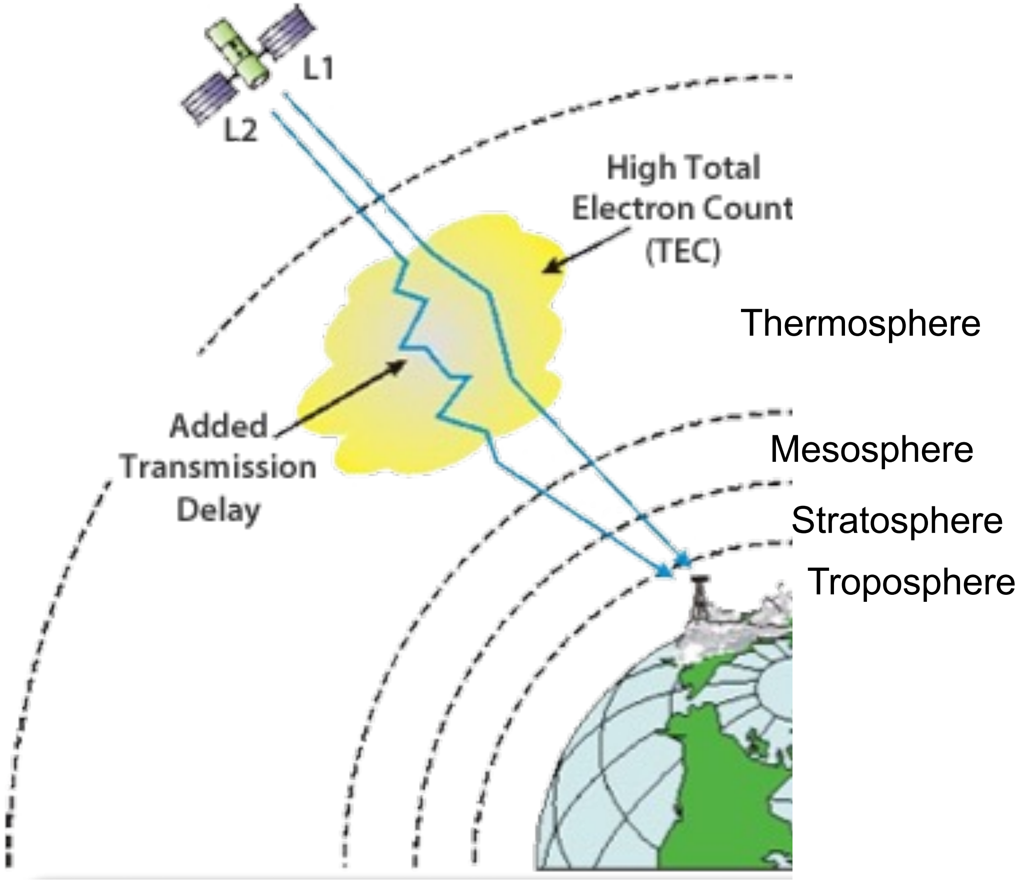

https://spotlight.unavco.org/how-gps-works/gps-basics/gps-and-geosciences.html

Total Electron Content (TEC)

GNSS dual-frequency observations allow the estimation of ionospheric TEC variations.

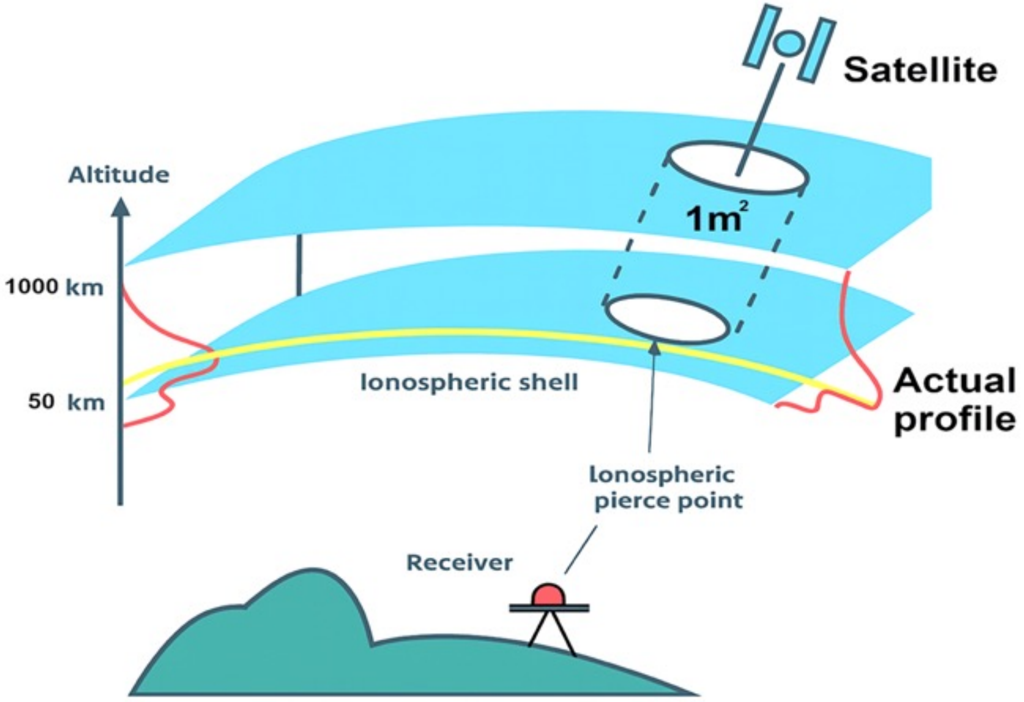

Kenpankho (2006)

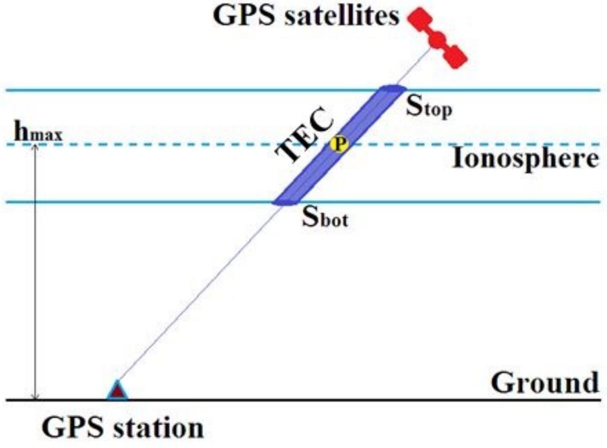

The total electron content *I* is the electron density *Ne* integrated along a beam:

$$I = \int_{Sbot}^{Stop} N_e \, ds$$

TEC calculation using the phase measurements at two GNSS frequencies:

$$I = \frac{1}{40.308} \frac{f_1^{\,2} f_2^{\,2}}{f_1^{\,2} - f_2^{\,2}} \left[(L_1\lambda_1 - L_2\lambda_2) + const_{1,2} + \sigma L \right]$$

where $L_1\lambda_1$ и $L_2\lambda_2$ is the phase path increments of the radio signals; $L_1 = \frac{\Delta\varphi}{2\pi}$ and $L_2 = \frac{\Delta\varphi}{2\pi}$, phase measurements by GNSS-receiver made at frequencies of f_1 and f_2; $const_{1,2}$, ambiguity of phase measurements; σL, phase measurement error.

Baikal School, 2015 2

TEC variations can be used to monitor ionospheric disturbances generated by natural hazards.

IGS 2026 WORKSHOP
SANTIAGO DE CHILE
33°26′ S 70°39′ O

GNSS-TEC Detection Methodology

GNSS-TEC Detection Methodology

GNSS observations	RINEX files from IGS (International), CSN (Chile), RAMSAC (Argentine), RBMC (Brazil), LISN (Peru)
TEC estimation	Gopi Seemala method (Seemala and Valladares, 2011)
Detrending / Filtering	10th-order polynomial fit and band-pass filtering between 0.5 and 5 mHz. (Artru et al., 2005; Rolland et al., 2010; Galvan et al., 2011)
Detection of ionospheric disturbances	Hodochrones analysis

GNSS-TEC Detection Methodology

GNSS observations

RINEX files from IGS (International), CSN (Chile), RAMSAC (Argentine), RBMC (Brazil), LISN (Peru)

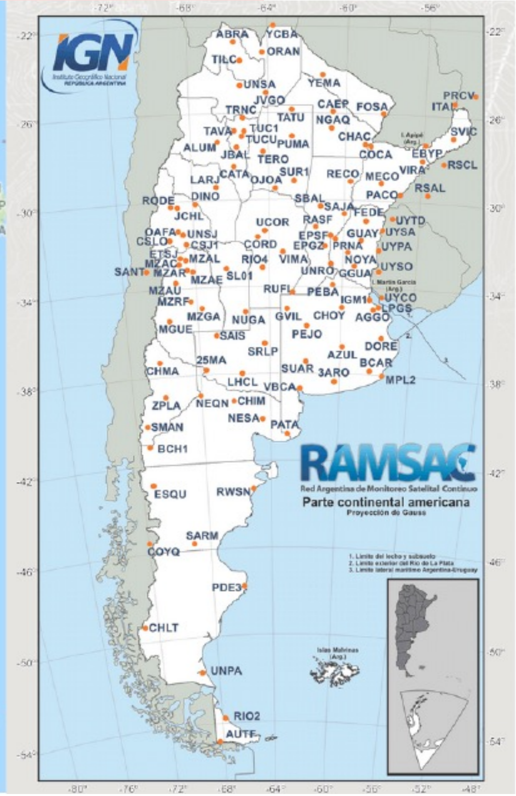

GNSS-TEC Detection Methodology

GNSS observations	RINEX files from IGS (International), CSN (Chile), RAMSAC (Argentine), RBMC (Brazil), LISN (Peru)
TEC estimation	Gopi Seemala method (Seemala and Valladares, 2011)
Detrending / Filtering	10th-order polynomial fit and band-pass filtering between 0.5 and 5 mHz. (Artru et al., 2005; Rolland et al., 2010; Galvan et al., 2011)
Detection of ionospheric disturbances	Hodochrones analysis

GNSS-TEC Detection Methodology

Bravo et al. (2022)

GNSS observations	RINEX files from IGS RBMC (Brazil), LISN
TEC estimation	Gopi Seemala meth
Detrending / Filtering	10th-order polynomi (Artru et al., 2005; R
Detection of ionospheric disturbances	Hodochrones analys

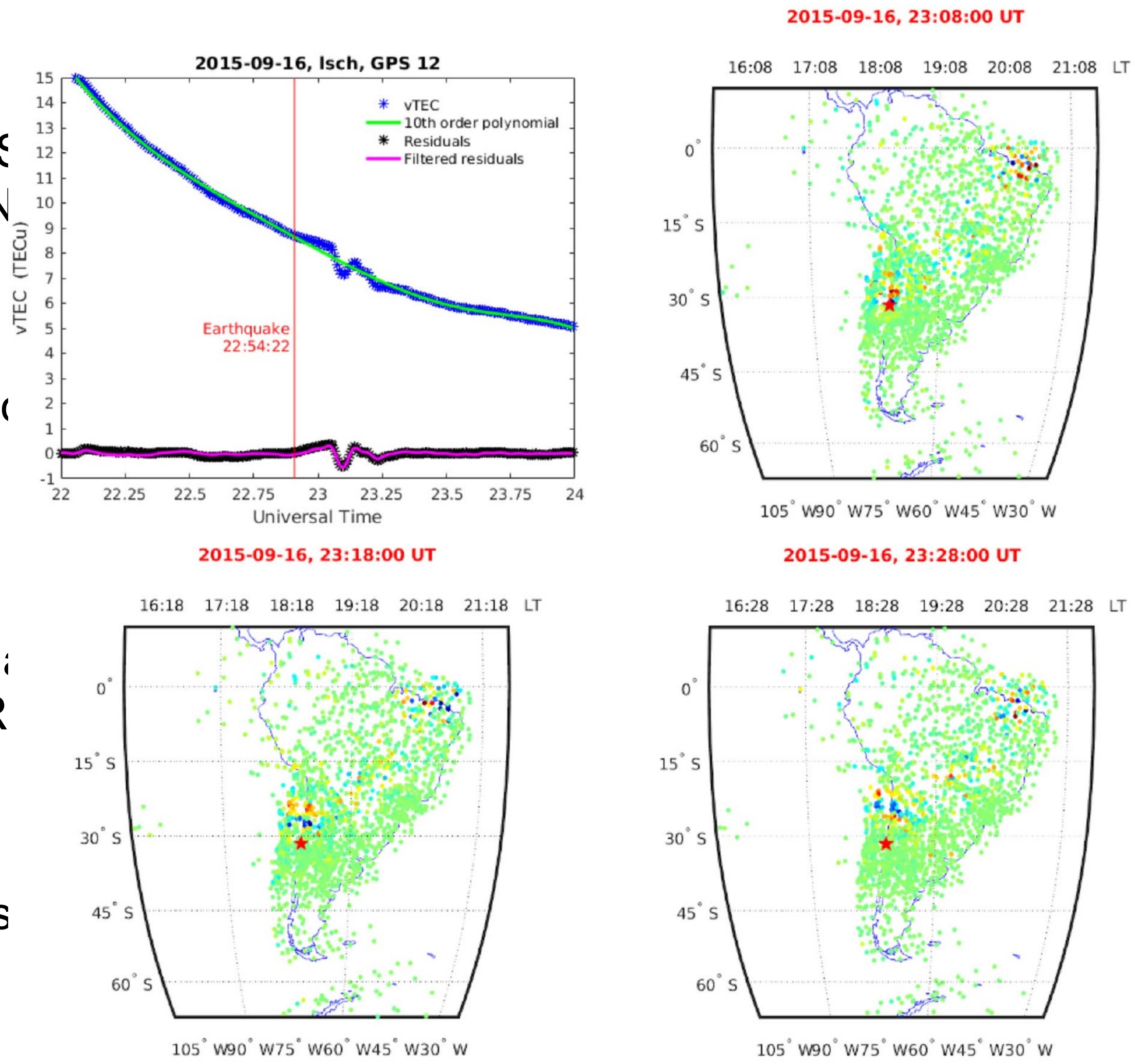

GNSS-TEC Detection Methodology

GNSS observations	RINEX files from IGS (International), CSN (Chile), RAMSAC (Argentine), RBMC (Brazil), LISN (Peru)
TEC estimation	Gopi Seemala method (Seemala & Valladares, 2011)
Detrending / Filtering	10th-order polynomial fit and band-pass filtering between 0.5 and 5 mHz. (Artru et al., 2005; Rolland et al., 2010; Galvan et al., 2011)
Detection of ionospheric disturbances	Hodochrones analysis

dology

Bravo et al. (2022)

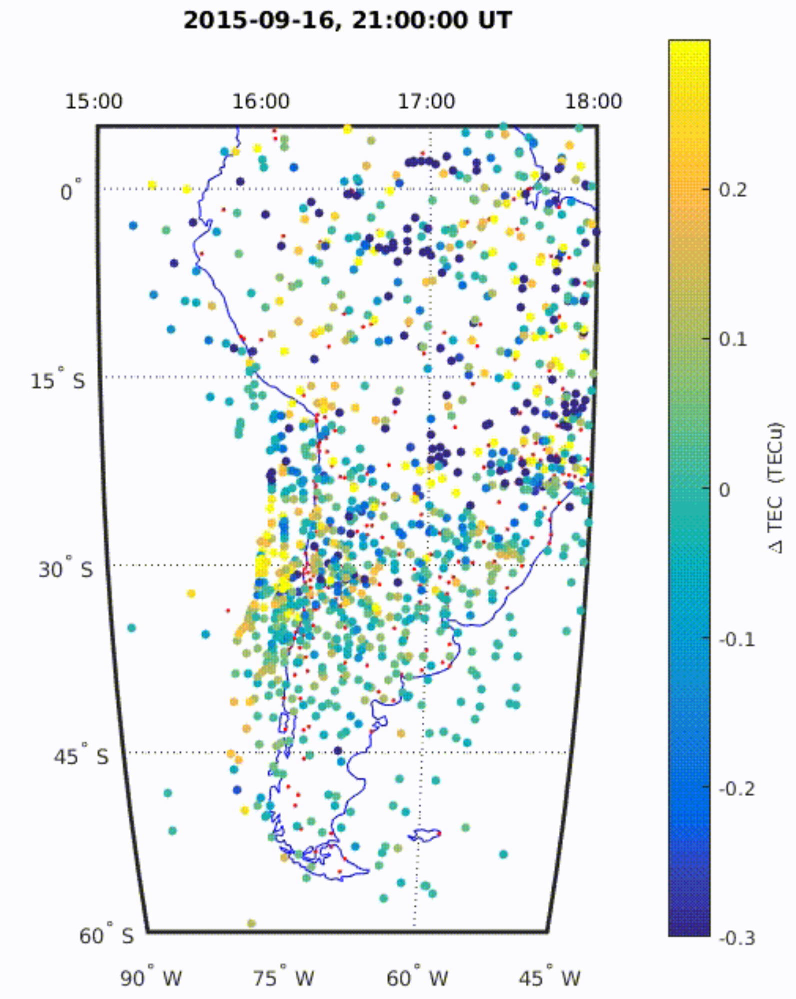

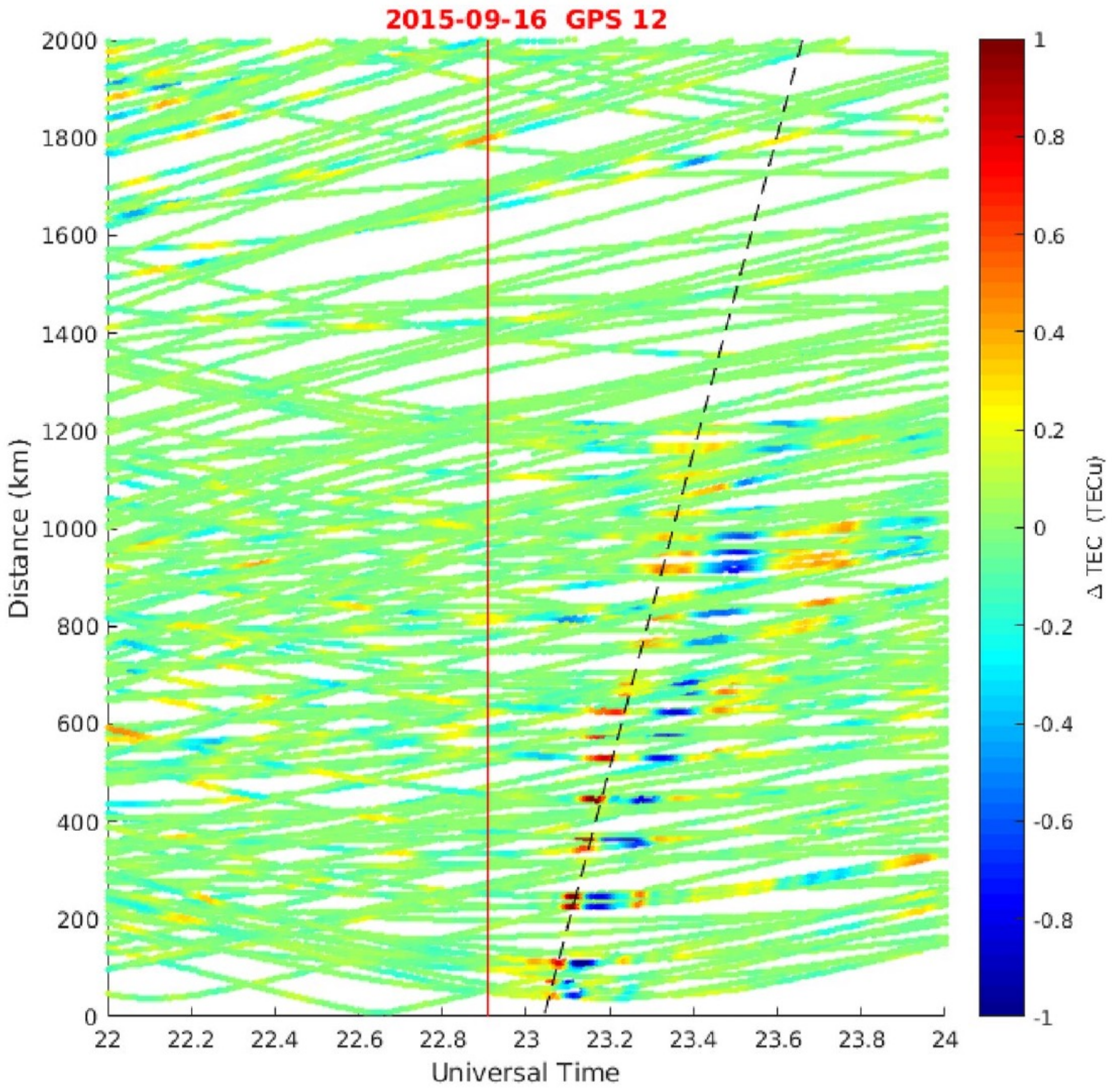

IGS 2026 WORKSHOP
SANTIAGO DE CHILE
33°26' S 70°39' O

Results: Observed Traveling Ionospheric Disturbances (TIDs)

Results: Observed Traveling Ionospheric Disturbances (TIDs)

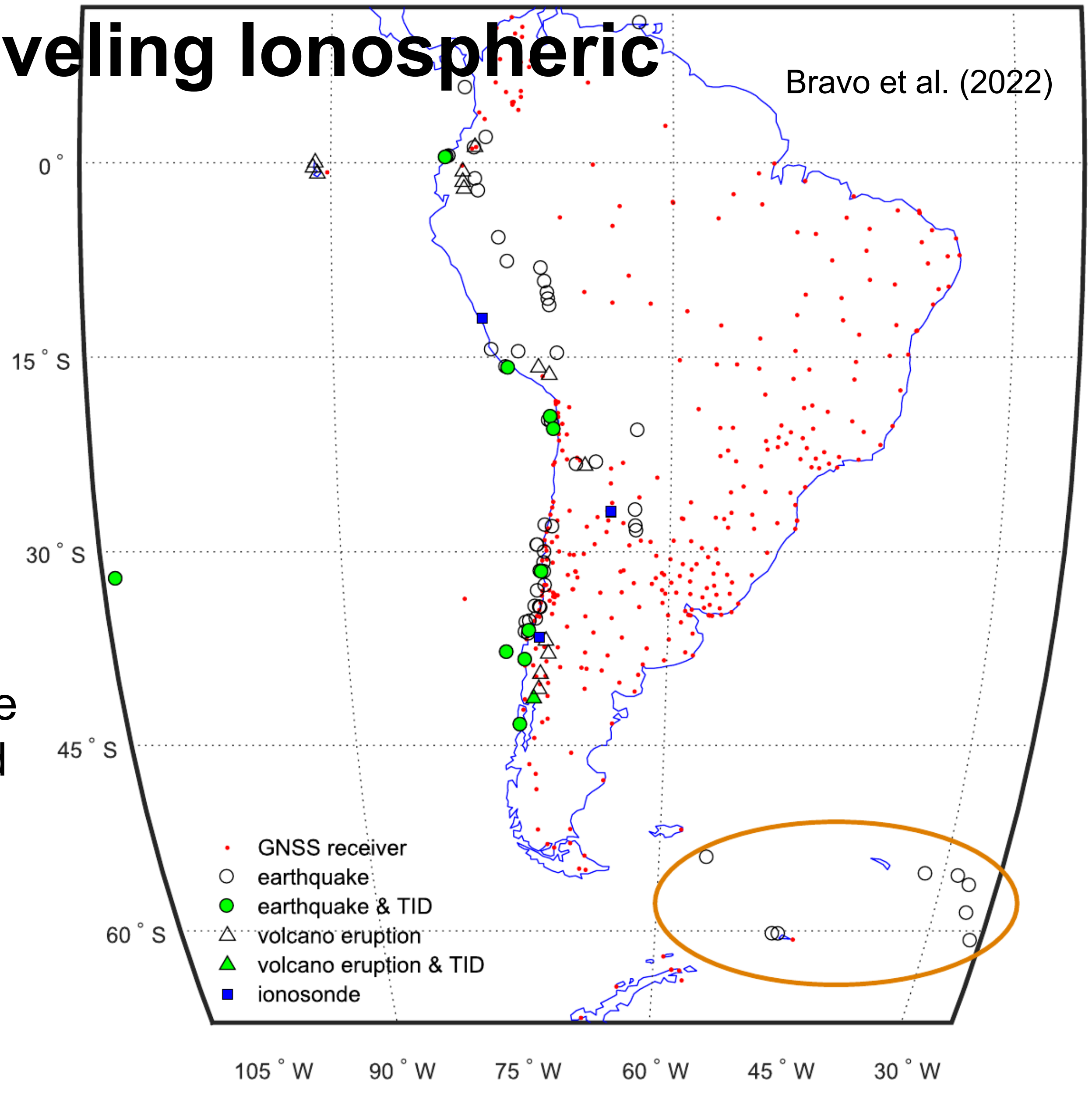

Events in South America between 2010 and 2020 were selected considering only earthquakes with **Mw ≥ 6.7** and volcanic eruptions with **VEI ≥ 2**, resulting in a database of **63** earthquakes and **20** eruptions.

Filled symbols indicate events for which Traveling Ionospheric Disturbances (TIDs) were detected, corresponding to **10** earthquakes and **2** volcanic eruptions.

Year	Date	UT	Latitude (°)	Longitude (°)	Magnetic inclination (°)	Depth (km)	Mag. (M_w)	Type of rupture	Tsunami height (m)	Daily Ap index	Observed TID (PRN)	Direction	Speed (m/s)	Amp. max (TECu)	Delay (min)	Range (km)	Publications
2010	Feb 27	06:34:12	-36.122	-72.898	-37.1	23	8.8	reverse	29.00	1	11, 13, 20, 23 11, 13,17, 20, 23, 31	N-E N-S-E-W	~2500 ~1000	~1.4	~6	~1200 ~2000	Rolland et al., 2010 Galvan et al., 2011 Kakinami et al., 2012 Astafyeva et al., 2013 Perevalova et al., 2014 Grawe & Makela, 2015 Kamogawa et al., 2016 Maruyama et al., 2016a, 2016b, 2017 Reddy et al., 2015 Pulinets et al., 2019
		08:01:23	-37.773	-75.048	-38.9	35	7.4	normal			4, 13, 23	N-S-E	~1000	~0.1	~9	~600	Perevalova et al., 2014 Reddy et al., 2015
	Mar 11	14:39:44	-34.290	-71.891	-35.1	11	6.9	normal	0.14	10	-						
		14:55:28	-34.326	-71.799	-35.1	18	7.0	normal									
	Mar 16	02:21:58	-36.217	-73.257	-37.2	18	6.7	reverse	-	4	-						
	Aug 12	11:54:16	-1.266	-77.306	20.0	207	7.1	normal	-	4	-						
2011	Jan 01	09:56:58	-26.803	-63.136	-27.7	577	7.0	normal	-	4	-						
	Jan 02	20:20:18	-38.355	-73.326	-39.4	24	7.2	reverse	-	4	4, 14	N-W	~1400	~0.2	~10	~400	
	Feb 11	20:05:31	-36.355	-72.960	-37.4	26	6.9	reverse	0.15	5	-						
	Feb 14	03:40:10	-35.380	-72.834	-36.3	21	6.7	reverse	-	13	-						
	Aug 24	17:46:12	-7.641	-74.525	8.1	147	7.0	normal, minor strike-slip comp	-	7	-						
	Sep 02	13:47:09	-28.398	-63.029	-30.0	579	6.7	normal, minor strike-slip comp	-	3	-						
	Oct 28	18:54:34	-14.438	-75.966	-4.4	24	6.9	reverse	-	0	-						
2012	Mar 25	22:37:06	-35.200	-72.217	-36.2	41	7.1	reverse	-	4	-						
	Apr 17	03:50:16	-32.625	-71.365	-33.4	29	6.7	reverse	-	9	-						

	May 28	05:07:23	-28.043	-63.094	-29.6	587	6.7	normal, major strike-slip comp	-	4	-						
	Sep 30	16:31:36	1.929	-76.362	24.8	170	7.3	normal	-	13	-						
2013	Jan 30	20:15:43	-28.094	-70.653	-27.7	45	6.8	reverse, minor strike-slip comp	-	1	-						
	Feb 09	14:16:08	1.135	-77.393	23.6	145	6.9	strike slip	-	3	-						
	Jul 15	14:03:40	-60.857	-25.070	-59.0	11	7.3	strike slip, minor normal comp	-	24	-						
	Aug 13	15:43:15	5.773	-78.200	30.8	12	6.7	reverse	-	8	-						
	Sep 25	16:42:43	-15.839	-74.511	-7.4	40	7.1	strike slip	-	4	2, 5, 7, 8, 10	N-W	~1200	~0.2	~10	~1000	
	Nov 16	03:34:31	-60.263	-47.062	-56.6	10	6.9	strike slip, major reverse comp	-	12	-						
	Nov 17	09:04:56	-60.274	-46.401	-56.7	10	7.7	strike slip	0.15	6	-						
	Nov 25	06:27:33	-53.945	-55.003	-52.7	12	7.0	reverse, minor strike-slip comp	-	0	-						
2014	Mar 16	21:16:30	-19.981	-70.702	-15.4	20	6.7	reverse	0.26	1	-						
	Apr 01	23:46:47	-19.610	-70.769	-14.7	25	8.2	reverse	4.63	5	1, 11, 13, 17, 20, 23 4, 10, 17, 20, 23	N-S-E-W S-E-W	~1000 ~240	~1.5 ~0.3	~9 ~60	~2200 800-2600	Reddy et al., 2015 Shrivastava et al., 2021
		23:57:59	-19.893	-70.946	-15.2	28	6.9	reverse			-						
	Apr 03	02:43:13	-20.571	-70.493	-16.4	22	7.7	reverse, major strike-slip comp	0.74	5	4, 7, 8, 9, 13, 23 5	N-S-E-W S-W	~1000 ~190	~0.8 ~0.2	~9 ~90	~800 1200-1600	
	Jun 29	07:52:55	-55.47	-28.367	-58.1	8	6.9	normal	-	6	-						
	Aug 24	23:21:46	-14.598	-73.571	-5.4	101	6.8	reverse	-	2	-						
	Oct 09	02:14:31	-32.108	-110.811	-42.2	17	7.0	normal	0.47	13	3, 16, 21	N-E	~1100	~0.3	~9	~800	
2015	Feb 11	18:57:22	-23.113	-66.688	-21.8	223	6.7	reverse	-	5	-						
	Sep 16	22:54:22	-31.573	-71.674	-32.4	22	8.3	reverse	13.6	11	2, 12, 14, 24, 25, 29	N-S-E-W	~900	~1.2	~9	~1800	Reddy et al., 2016 Kamogawa et al., 2016 Grawe & Makela, 2017 Berngardt et al., 2017 Ravanelli et al., 2021 Shrivastava et al., 2021
		23:18:42	-31.562	-71.426	-32.4	28	7.0	reverse			-						
	Sep 17	04:10:28	-31.517	-71.804	-32.3	23	6.7	reverse	-	10	-						
	Nov 07	07:31:44	-30.880	-71.452	-31.6	46	6.8	reverse	-	38	-						
	Nov 11	01:54:39	-29.507	-72.007	-29.8	12	6.9	reverse	0.55	22	-						
		02:46:20	-29.510	-72.059	-29.8	10	6.9	normal			-						

	Nov 24	22:45:39	-10.537	-70.944	1.2	606	7.6	normal	-	0	-						
		22:50:54	-10.060	-71.018	2.1	620	7.6	normal			-						
	Nov 26	05:45:18	-9.183	-71.257	3.7	603	6.7	reverse, minor strike-slip comp	-	1	-						
2016	Apr 16	23:58:37	0.382	-79.922	22.0	21	7.8	reverse, minor strike-slip comp	0.5	11	6, 7, 17, 30	S-E-W	~1200	~1.0	~9	~500	Berngardt et al., 2017
	May 18	07:57:03	0.426	-79.790	22.1	16	6.7	reverse, minor strike-slip comp	-	7	-						
		16:43:44	0.495	-79.616	22.2	30	6.9	normal, major strike-slip comp	-	7	-						
	May 28	09:47:00	-56.241	-26.935	-58.4	78	7.2	reverse	-	13	-						
	Aug 19	07:32:23	-55.285	-31.877	-57.6	10	7.4	reverse	0.10	4	-						
	Dec 25	14:22:27	-43.406	-73.941	-44.3	38	7.6	reverse	0.44	20	12, 24 2, 6, 29	N-E-W N-E-W	~1100 ~200	~0.3 ~0.15	~9 ~90	~600 1000-1600	
2017	Apr 24	21:38:31	-33.038	-72.062	-34.3	28	6.9	reverse	0.16	19	-						
2018	Jan 14	09:18:46	-15.768	-74.709	-7.9	39	7.1	normal	0.15	13	-						
	Apr 02	13:40:35	-20.659	-63.006	-20.7	559	6.8	reverse, major strike-slip comp	-	4	-						
	Aug 21	21:31:48	10.773	-62.902	31.5	147	7.3	normal	-	7	-						
	Aug 24	09:04:08	-11.036	-70.828	-0.4	630	7.1	reverse, major strike-slip comp	-	4	-						
	Dec 11	02:26:29	-58.545	-26.386	-58.7	133	7.1	normal	-	8	-						
2019	Jan 05	19:25:39	-8.144	-71.587	5.0	570	6.8	normal	-	16	-						
	Jan 20	01:32:52	-30.040	-71.382	-31.0	63	6.7	normal, minor strike-slip comp	-	3	-						
	Feb 22	10:17:24	-2.186	-77.051	17.0	145	7.5	normal, major strike-slip comp	-	3	-						
	Mar 01	08:50:43	-14.713	-70.155	-7.4	267	7.0	normal	-	23	-						
	May 26	07:41:15	-5.812	-75.270	10.2	123	8.0	reverse	-	4	-						
	Aug 01	18:28:07	-34.236	-72.310	-35.9	25	6.8	reverse	-	7	-						
	Sep 29	15:57:53	-35.476	-73.163	-37.2	11	6.7	normal	-	12	-						
2020	Jun 03	07:35:36	-23.282	-68.472	-22.5	112	6.8	reverse	-	3	-						
	Sep 01	04:09:28	-27.971	-71.309	-28.5	21	6.8	strike slip	-	18	-						

IGS 2026
WORKSHOP
SANTIAGO DE CHILE
33°26' S 70°39' O

Table 2
Information of Selected Volcanic Eruptions in South America Between 2010 and 2020 Time Interval With VEI ≥ 2, According to the GPV (https://volcano.si.edu/)

Year	Date	UT	Latitude (°)	Longitude (°)	Magnetic inclination (°)	Volcano	Mag. (VEI)	Type of eruption	Daily Ap index	Observed TID (PRN)	Direction	Speed (m/s)	Amp. max (TECu)	Delay (min)	Range (km)	Publications
2010	August 25	9:00	1.220	−77.370	24.1	Galeras	2	N/I	18	-						
2011	June 4	18:15	−40.590	−72.117	−41.5	Puyehue-Cordon Caulle	5	Plinian	13	-						
	November 27	22:01	−1.467	−78.442	19.4	Tungurahua	3	N/I	6	-						
2012	December 22	12:45	−37.863	−71.172	−39.1	Copahue	2	Freatica	1	-						
2013	January 25	17:10	−2.005	−78.341	18.3	Sangay	2	N/I	6	-						
	September 02	03:46	−16.355	−70.903	−8.9	Ubinas	2	N/I	9	-						
2015	March 03	06:01	−39.420	−71.939	−40.7	Villarica	2	Strombolian	10	-						
	March 17	23:56							108	-						
	April 22	21:04	−41.330	−72.618	−42.4	Calbuco	4	Subplinian	10	1, 3, 6, 9, 17, 23, 32	N-S-E-W	~1,100	~0.5	~30	~700	Miller et al. (2015) Shults et al. (2016) X. Liu et al. (2017) Aoyama et al. (2016)
	April 23	04:00							6	13, 15, 28	N-E-W	~1,200	~0.2	~40	~700	Shults et al. (2016) X. Liu et al. (2017)
	May 25	06:58	0.020	−91.350	19.7	Wolf	4	N/I	2	-						
	August 15	09:02	−0.677	−78.436	20.2	Cotopaxi	2	Phreatic	35	-						
	October 30	12:32	−23.370	−67.730	−22.0	Lascar	2	N/I	8	-						
2016	January 08	20:55	−36.868	−71.378	−38.4	Nevados de Chillán	2	Phreatic	7	-						
	November 07	01:40	−15.787	−71.857	−8.3	Sabancaya	3	N/I	3	-						
2017	September 04	18:25	−0.370	−91.550	18.8	Fernandina	2	N/I	16	-						
2018	June 26	19:40	−0.830	−91.170	18.1	Sierra Negra	2	N/I	20	-						
	August 08	~20:00	−2.005	−78.341	17.5	Sangay	2	N/I	4	-						
2019	March 26	11:15	−2.005	−78.341	17.4	Sangay	2	N/I	4	-						
	June 24	12:00	−16.355	−70.903	−10.1	Ubinas	2	N/I	4	-						

Results: Observed Traveling Ionospheric Disturbances (TIDs)

Events in South America between 2010 and 2020 were selected considering only earthquakes with **Mw ≥ 6.7** and volcanic eruptions with **VEI ≥ 2**, resulting in a database of **63** earthquakes and **20** eruptions.

Filled symbols indicate events for which Traveling Ionospheric Disturbances (TIDs) were detected, corresponding to **10** earthquakes and **2** volcanic eruptions.

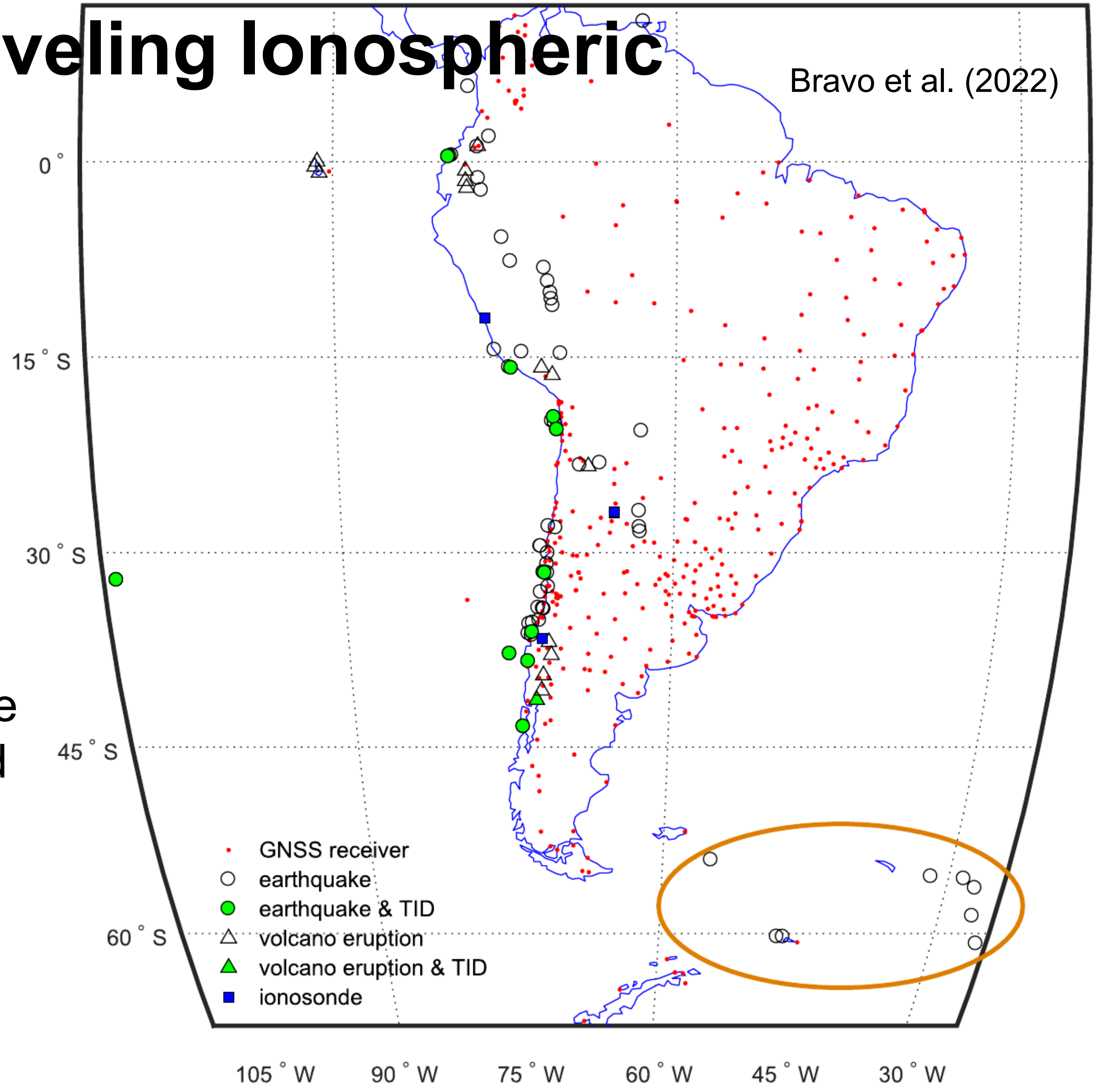

Bravo et al. (2022)

IGS 2026 WORKSHOP
SANTIAGO DE CHILE
33°26' S 70°39' O

Results: Observed Traveling Ionospheric Disturbances (TIDs)

Bravo et al. (2022)

a) A fast perturbation (~2400 m/s), possibly associated with Rayleigh surface waves, together with the characteristic acoustic-wave signature (~1000 m/s). The vertical red line indicates the earthquake origin time.

b) Resonant ionospheric disturbance associated with the 2015 Calbuco Volcano eruption.

c) Acoustic- and gravity-wave-like ionospheric disturbances, the latter possibly associated with a tsunami. Artifacts related to the Seemala method are also visible due to the UT day transition.

d) Weak ionospheric signature associated with the 2014 Easter Island earthquake event, likely due to sparse nearby GNSS coverage.

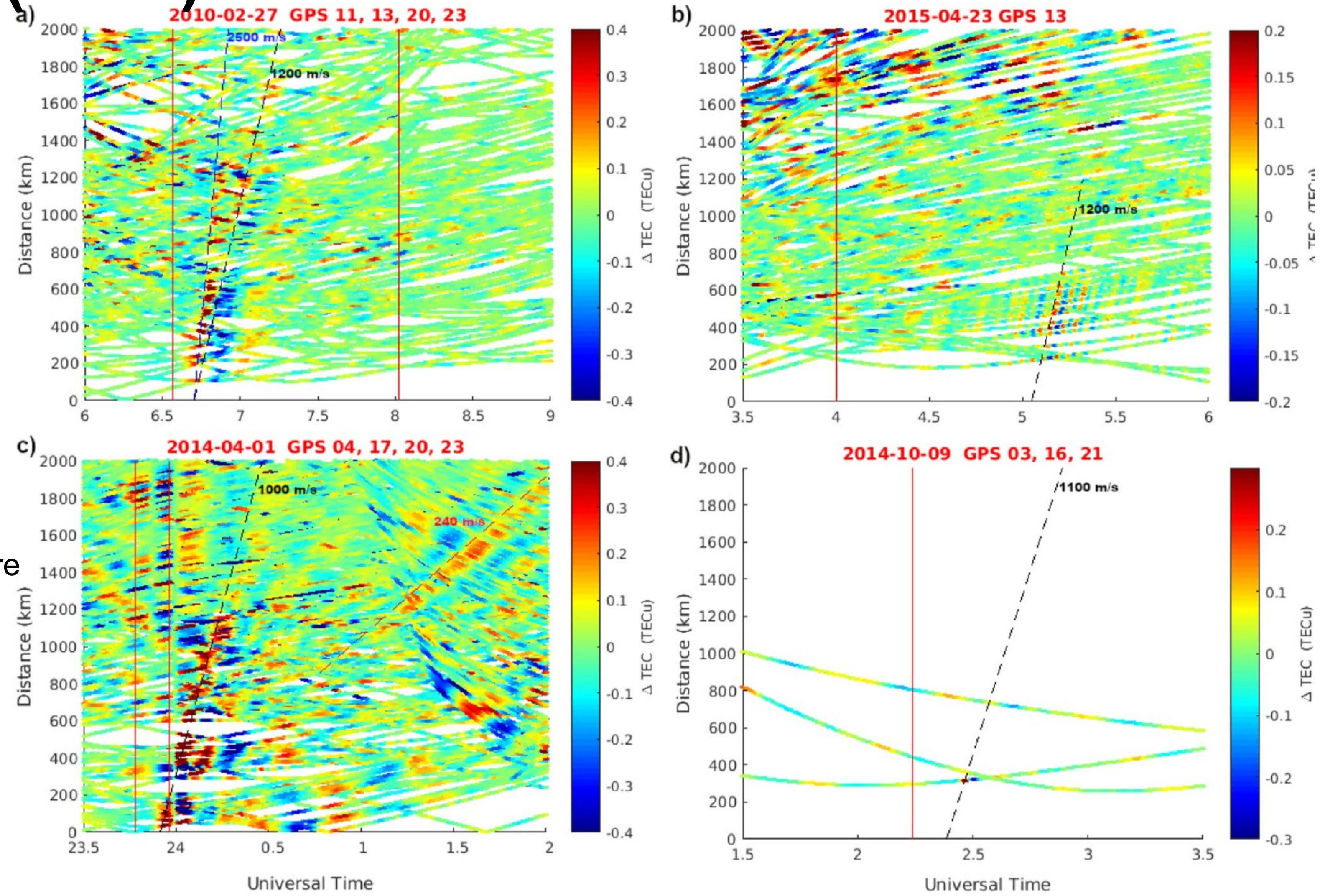

Results: Observed Traveling Ionospheric Disturbances (TIDs)

Bravo et al. (2022)

(a) and (b) show the same ionospheric disturbance observed to the north and south, respectively, revealing a predominant northward propagation in the Southern Hemisphere (related to upward propagation along geomagnetic field lines).

(c) and (d) show another event where no clear disturbance is observed to the east, while a weak signature is detected to the west (possibly associated with the Andes Mountains?).

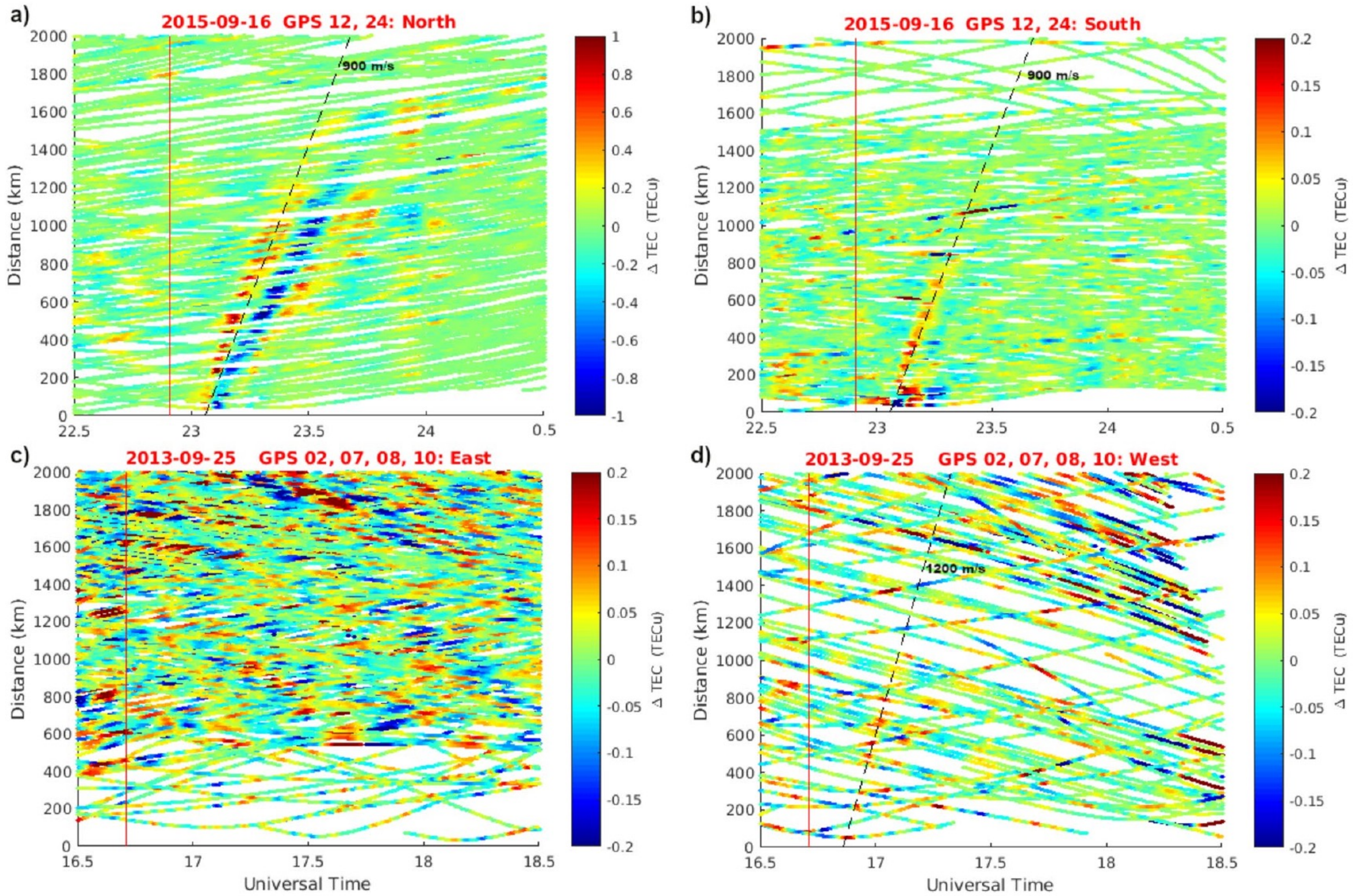

Results: Spectral characteristics of ionospheric disturbances (wavelet analysis)

Bravo et al. (2022)

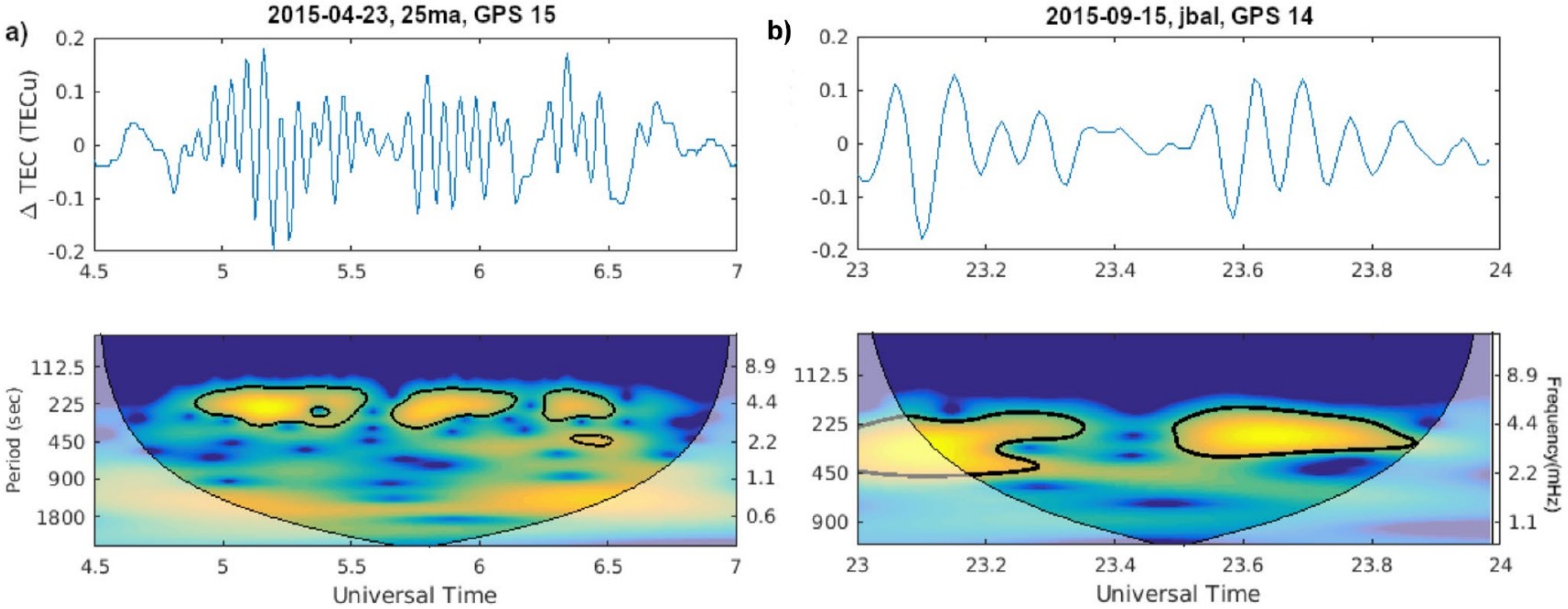

(a) The 2015 Calbuco Volcano eruption shows resonant oscillations with dominant periodicities centered around ~200 s.

(b) Earthquake-induced TIDs exhibit dominant periodicities centered around ~300 s, consistent with acoustic-gravity wave dynamics.

Results: Regression analysis of ionospheric disturbance parameters

Bravo et al. (2022)

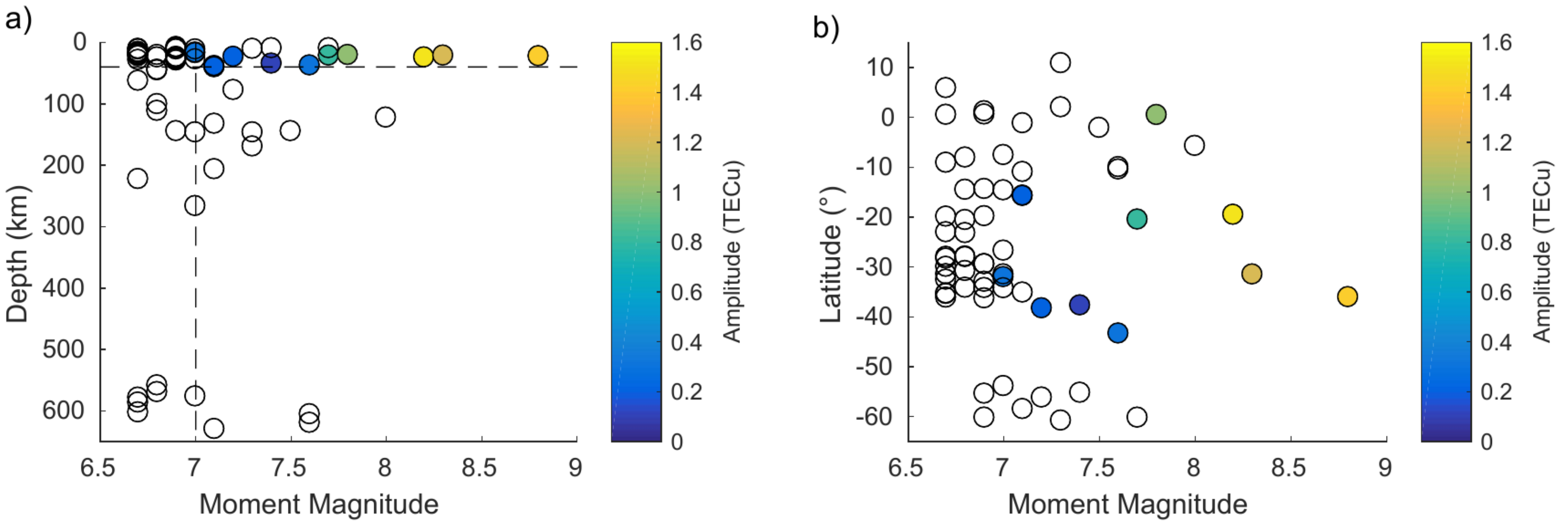

(a) Depth vs magnitude shows that TEC disturbances are mainly observed for events with Mw ≥ 7, while affected events are generally shallower than ~40 km.

(b) Latitude vs magnitude shows that events associated with TEC disturbances are located north of ~45°S.

Results: Regression analysis of ionospheric disturbance parameters

Bravo et al. (2022)

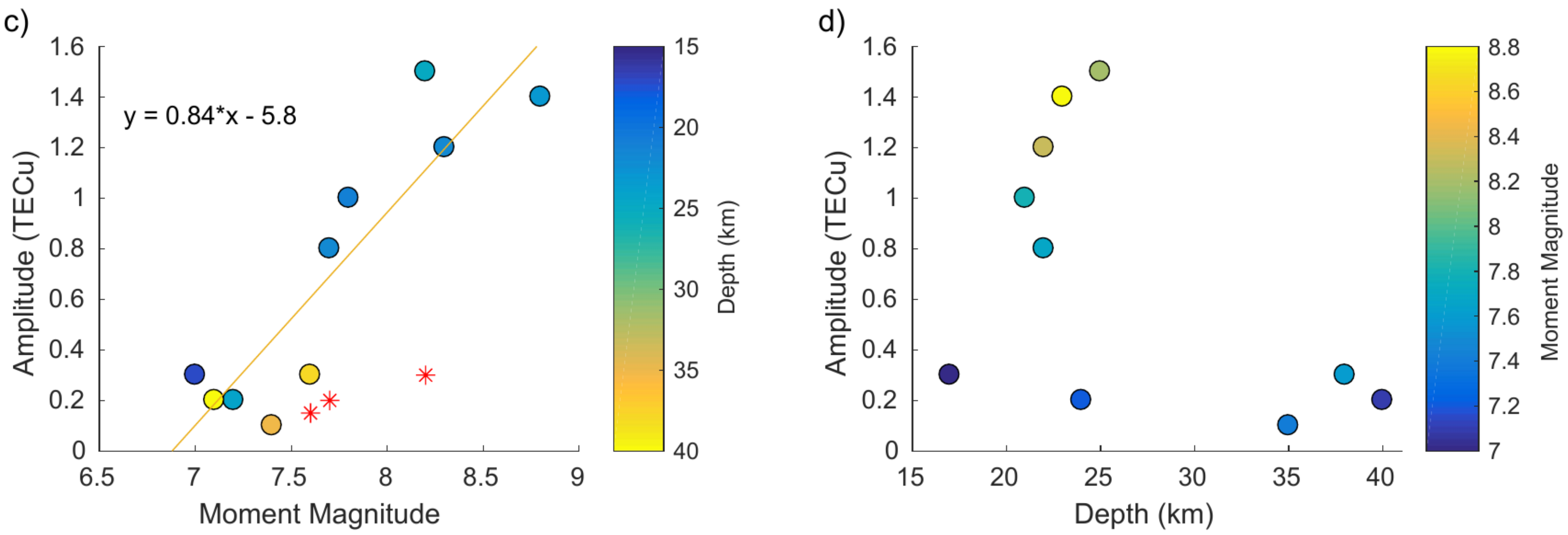

(c) TID amplitude vs magnitude shows an approximately linear relationship for the acoustic-wave component, while the gravity-wave trend is less certain due to the limited number of points

(d) TID amplitude vs depth shows no clear relationship between disturbance amplitude and event depth.

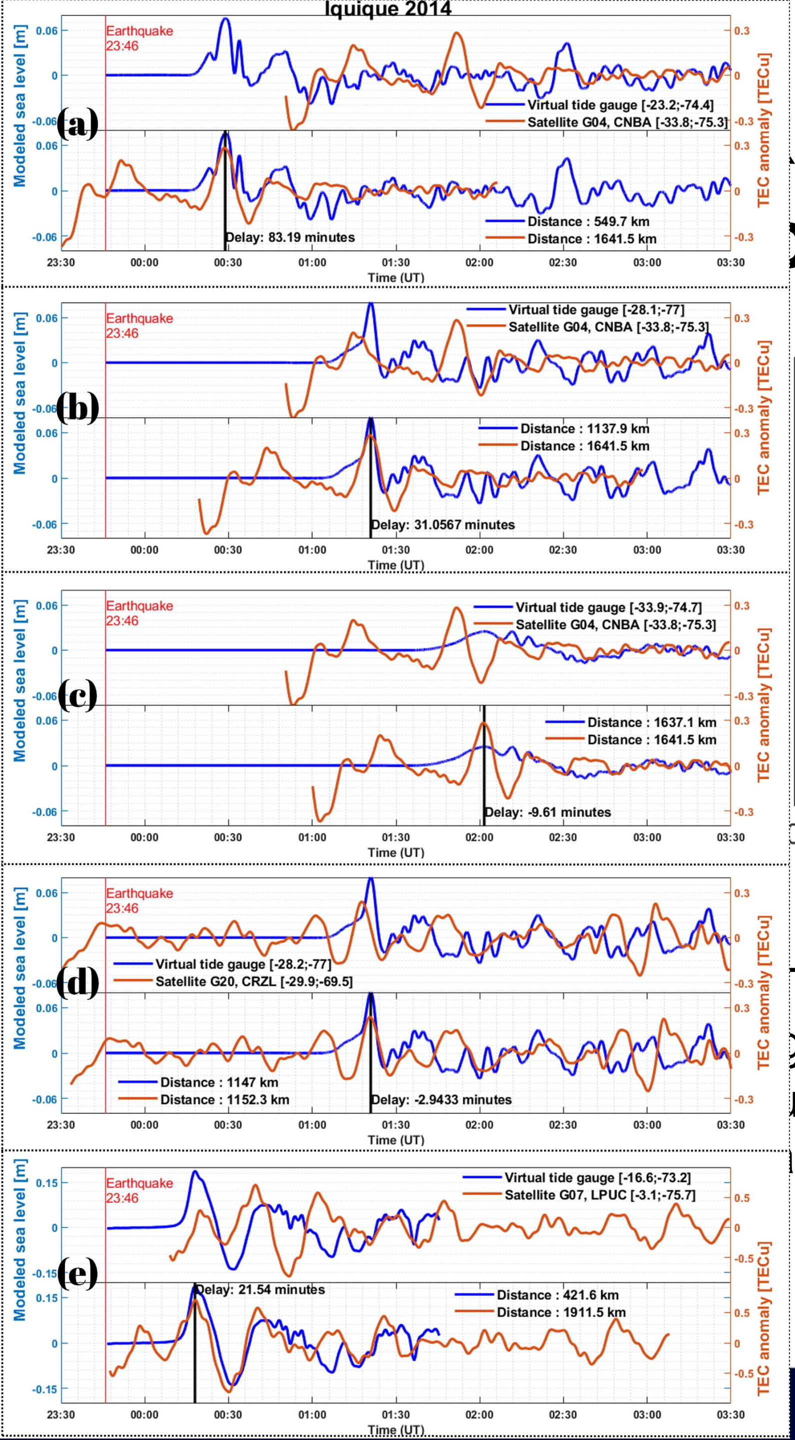

egression analysis of ionospheric ce parameters

Bravo et al. (2022)

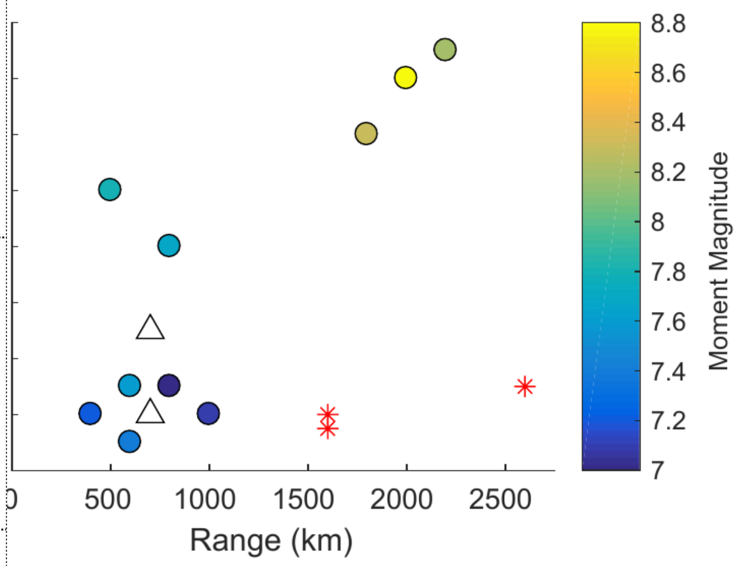

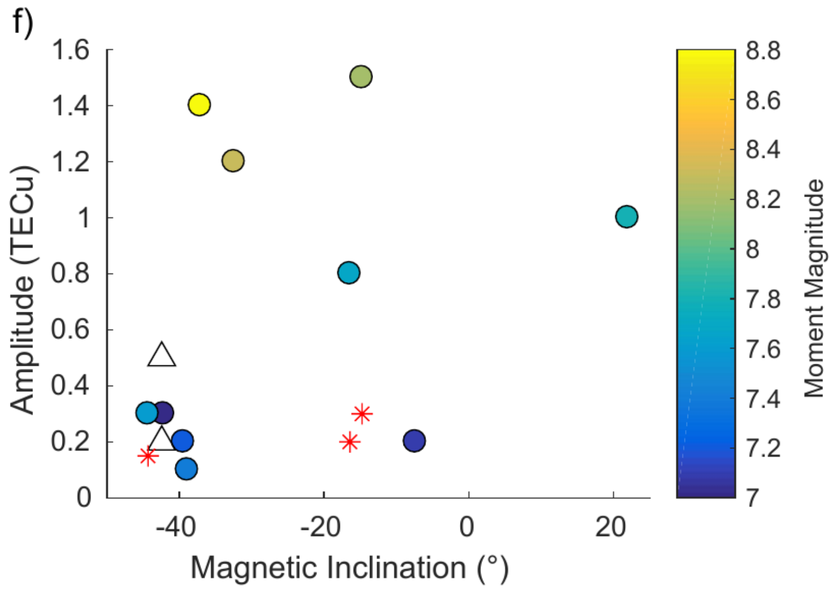

TID amplitude vs propagation range gests that larger-amplitude urbances tend to propagate over ter distances.

(e) Latitude vs magnetic inclination shows no clear association with TID occurrence or amplitude.

Castillo-Rivera et al. (2025)

IGS 2026 WORKSHOP

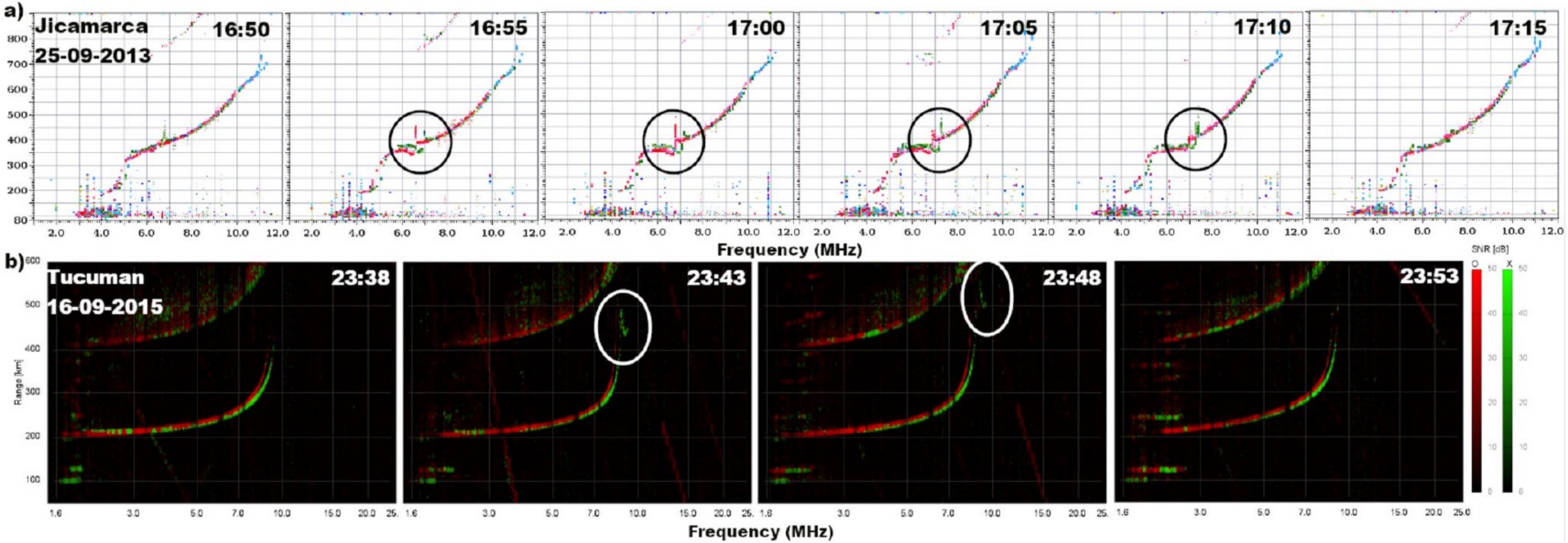

Perturbations of vertical distribution of electronic concentration derived from ionosonde observations. (a) Jicamarca's (12.0°S; 76.8°W) cusp ionogram sequence after 25 September 2013 Peru (15.8°S; 74.5°W) earthquake. (b) Tucuman's (26.9°S; 65.4°W) F3 layer ionogram sequence after 16 September 2015 Illapel (31.6°S; 71.7°W) earthquake.

Conclusions

GNSS-derived TEC observations successfully detect ionospheric disturbances associated with earthquakes, tsunamis, and volcanic eruptions in South America.

Detected Traveling Ionospheric Disturbances (TIDs) exhibit propagation patterns consistent with atmospheric acoustic and gravity wave dynamics, with characteristic spectral periodicities (~200–300 s).

A magnitude threshold (Mw $\gtrsim$ 7) and a focal depth constraint (typically shallower than ~40 km) are generally required for clear ionospheric detectability.

However, some events exceeding Mw ≥ 7 do not produce detectable TIDs when occurring at larger depths, highlighting the strong control of focal depth on lithosphere–atmosphere–ionosphere coupling.

Conclusions

Among the events satisfying both Mw ≥ 7 and depth < 40 km, most correspond to strike-slip faulting and are predominantly located in the Scotia Plate region, suggesting a possible tectonic control on ionospheric coupling efficiency.

TID amplitude shows a clear linear relationship with earthquake magnitude and increases with propagation range, indicating a systematic scaling of ionospheric response with event energy and spatial extent.

Five of the ten earthquake-associated TID cases identified in this study have been previously reported, and both volcanic eruption cases are consistent with earlier documented ionospheric responses, supporting the robustness of the results.

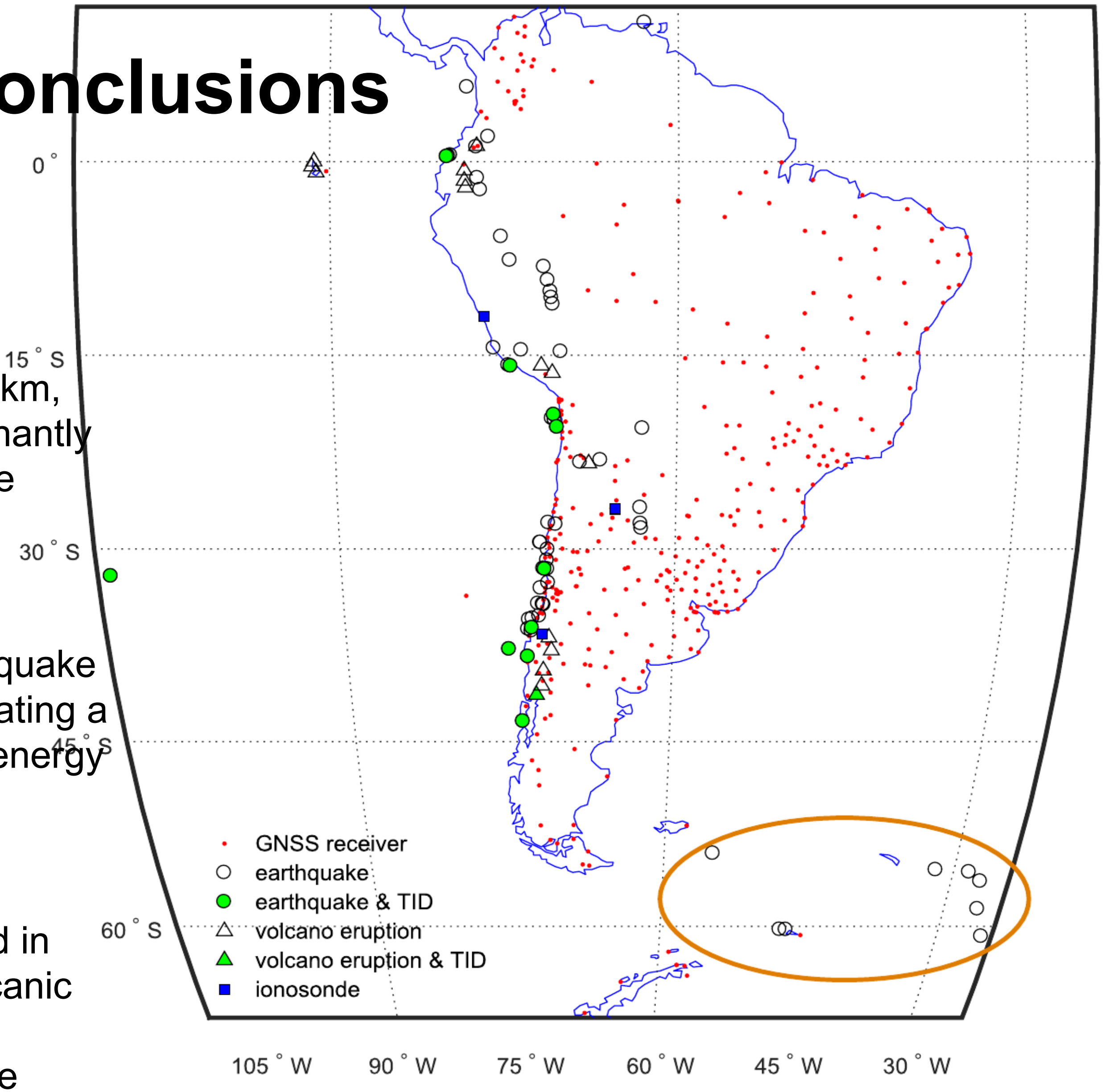

IGS 2026 WORKSHOP
SANTIAGO DE CHILE
33°26′ S 70°39′ O

Thank you!!!

IGS 2026 WORKSHOP
SANTIAGO DE CHILE
33°26' S 70°39' O

References

- Artru, J., V. Ducic, H. Kanamori, P. Lognonné, and M. Murakami (2005), Ionospheric detection of gravity waves induced by tsunamis, Geophys. J. Int., 160, 840–848, doi:10.1111/j.1365-246X.2005.02552.x.
- Astafyeva, E. (2019). Ionospheric detection of natural hazards. Reviews of Geophysics, 57, 1265–1288 doi:10.1029/2019RG000668.
- Bravo, M, Benavente, R, Foppiano, A, Urra, B, & Ovalle, E (2022). Traveling Ionospheric Disturbances observed over South America after lithospheric events: 2010–2020. J. Geophys. Res. Space Physics, 127, e2021JA030060, doi:10.1029/2021JA030060
- Castillo-Rivera, C, Bravo, M, Calisto, I, González, J, Urra, B., Benavente, R, Foppiano, A, Figueroa, D, and Ovalle, E (2025). Detection of near- and far-field traveling ionospheric disturbances during Tsunami Events over South Pacific, Adv Space Res, 75(1), 1033-1051, doi:10.1016/j.asr.2024.10.020
- Galvan, D. A., Komjathy, A., Hickey, M. P., & Mannucci, A. J. (2011). The 2009 Samoa and 2010 Chile tsunamis as observed in the ionosphere using GPS total electron content. J Geophys Res, 116, A06318, doi:10.1029/2010JA016204
- Kenpankho, P. (2026) Ionospheric Precursors to Earthquakes: A Review of Mechanisms and Observations, Frontiers in Earthquake and Geohazard Research, doi:10.5772/intechopen.1013783
- Rolland, L. M., Vergnolle, M., Nocquet, J.-M., Sladen, A., Dessa, J.-X., Tavakoli, F., et al. (2013). Discriminating the tectonic and non-tectonic contributions in the ionospheric signature of the 2011, Mw 7.1, dip-slip Van earthquake, Eastern Turkey. Geophysical Research Letters, 40, 2518–2522, doi: 10.1002/grl.50544
- Seemala, G.K., Valladares, C.E., (2011). Statistics of total electron content depletions observed over the south american continent for the year 2008. Radio Science 46. doi:10.1029/2011RS004722